

Shapes and Appearances Reconstructions of Thin Film Objects

YOSHIE KOBAYASHI^{1,a)} TETSURO MORIMOTO^{2,b)} IMARI SATO^{3,c)} YASUHIRO MUKAIGAWA^{4,d)}
TAKAO TOMONO^{2,e)} KATSUSHI IKEUCHI^{1,f)}

Abstract: Modeling objects in real world is one of the important research topics in computer vision field. Such modeling results are widely used to games, movies and cultural heritage digitization to name a few. Among various reflection properties, interference is one of the most intractable effects since its color varies iridescence along the viewing and lighting directions. Yet, modeling shapes and appearances of objects with interference effects would be useful for diverse applications in industry, biology, archeology and medicine. The interference effects are due to interactions between incoming and reflected lights, and depend mainly on geometrical information and optical parameters. In this thesis, we propose a novel method to reconstruct shapes and estimate optical parameters of thin film objects. We also evaluate the effectiveness of our method in experiment.

1. Introduction

Appearance modeling of real world objects is an important research topic in computer graphics and computer vision fields. Such appearance modeling can be applied to games, movies and cultural heritage digitization for re-rendering object appearance quickly. Real-world objects have several reflectance properties such as scattering, absorption, diffraction, refraction and interference which influence their appearances. These properties interact each other and give the estimation process a challenge.

The interference effects caused by thin films belong to one of the most important effects in appearance modeling. Interference effects occur when a thin layer exists over an object surface. Thus, the effects are quite common in such objects as laminated film, soap bubble and oil film. The interference effects are, as the nature, due to interactions between incoming and reflected lights and depending on not only material characteristics but also geometric parameters. Therefore, once we can establish an estimation method from observed appearances, we can estimate material characteristics as well as geometric parameter. Thus, the method can be applied to many fields including industrial inspection, bi-

ological analysis, and archeology research.

Methods in computer graphics[12][11] showed that physics model can represent appearance of thin film interference effects well. Therefore, estimating parameters of the physics model is important to reconstruct appearance of thin film. In optics field, several methods exist for estimating parameters of the physics model which are refractive index and film thickness. Interference spectroscopy[18] and ellipsometry[1] are representative methods to estimate film thickness with known refractive index. Kitagawa [14], [15] proposed image based method, which utilizes RGB values along the film thickness, but the method needs known refractive index. Kobayashi *et al.* [16] proposed a method to estimate unknown refractive index and film thickness. The limitation of these methods is that they can be only applied to flat surfaces.

We propose methods to estimate shapes and appearances of thin film objects at once. Firstly, we use conventional RGB camera and focus on polarization and intensity along zenith angles. This method can reconstruct thin film objects easily, though it needs known refractive index of target objects. To handle thin film objects with unknown refractive index, we propose a method using hyper-spectral images. In this method, we focus on the peak intensity of reflectance spectra to reconstruct shapes. We minimize the least square between measured reflectance and model reflectance then determine optical parameters.

The rest of this paper is organized as follows. In Section 2, we discuss several existing methods of reconstructing shapes and appearances for various reflection properties. In Section 3, we describe a reflectance model of thin film objects. In Section 4, we propose a method to estimate shapes and appearances with RGB images. In Section 5, we conduct experiments by the method in Section 4 to evaluate the accuracy of our method. In Section 6, we propose a reconstruction method with spectral images. In

¹ The University of Tokyo, 7-3-1 Hongo, Bunkyo-ku, Tokyo 113-8656, Japan

² Toppan Printing Co. Ltd., 1-3-3 Suido, Bunkyo-ku, Tokyo 112-8531, Japan

³ National Institute of Informatics, 2-1-2 Hitotsubashi, Chiyoda-ku, Tokyo 101-8430, Japan

⁴ Nara Institute of Science and Technology, 8916-5 Takayama, Ikoma, Nara 630-0192, Japan

^{a)} yoshie@cvl.iis.u-tokyo.ac.jp

^{b)} tetsuro.morimoto@toppan.co.jp

^{c)} imarik@nii.ac.jp

^{d)} mukaigawa@is.naist.jp

^{e)} takao.tomonono@toppan.co.jp

^{f)} ki@cvl.iis.u-tokyo.ac.jp

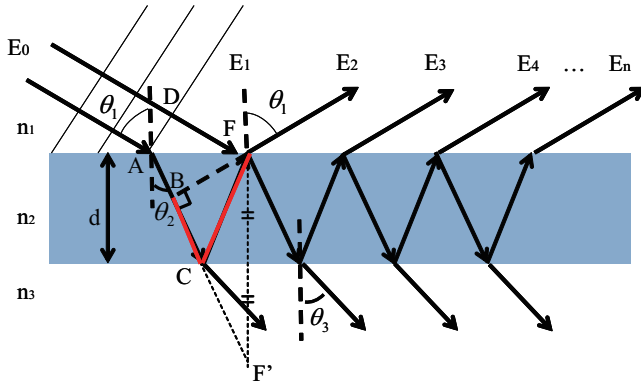


Fig. 1 Schematic diagram of thin film interference. n_1 , n_2 and n_3 are refractive index of incoming medium, thin film and outgoing medium respectively. θ_1 is zenith angle. θ_2 is refracting angle. θ_3 is angle of outgoing light transmitting the thin film.

Section 7, we demonstrate experiments to show the effectiveness of our method. In Section 8, we discuss errors of our methods in experiments. In Section 9, we summarize this paper and mention the future work.

2. Related Work

Various methods to acquire the appearances of objects in the real world have been proposed. In computer vision fields, appearances are defined by a bidirectional reflection distribution function (BRDF) that represents reflectance along the view and light directions. Holroyd et al. [8] and Dana et al. [3] constructed a BRDF look-up table in which they controlled the illumination and view directions by positioning the light, sensor, and sample sequentially. Mukaigawa et al. [22] and Dana et al. [4] have used an ellipsoidal mirror to measure the reflection of all directions at once. However, these methods are centered on reflection, which does not dramatically vary the appearance. It is thus difficult to apply these methods to thin film objects.

There are several methods to estimate shapes and appearances simultaneously. A representative method is the photometric stereo [5], which is applied to various reflectance properties such as diffusion, specularity, isotropy, and anisotropy. This method usually estimates shapes while fitting a reflectance model with captured images. However, when the reflectance of transparent objects is too complicated, this method does not work well. Several methods [27][24][19][20][21] have been proposed to estimate the shapes of transparent objects using polarization.

In computer graphics, there are several methods to render structural color caused by thin film, multiple films, refraction, and diffraction grating. Hirayama et al. [6], [7] have rendered multi-film interference focusing on a physical model while Sun et al. [25], [26] models the micro-structure of CDs precisely and reconstruct it realistically. Using the model of refraction among water droplets, Sadeghi et al. [23] have rendered a rainbow the same as a real images. Cuyppers et al. [2] uses the Wigner distribution function to model diffraction grating. They compare this model with reflectance from objects in the real world and show that it can represent the appearance as precisely as a physical model. Using a physical model, these methods can represent appearances well, but the model parameters need to be set manually, which

means we need to estimate the parameters of the physical model in order to reconstruct the thin film appearance well.

3. Reflectance Model of Thin Film Objects

In this section, we describe the appearance of thin film in RGB color space. Our method can be used with a regular digital camera. Observed RGB values are represented by integration of observed spectra. The observed spectrum is a multiplication of the camera sensitivity, reflectance, and illumination spectrum in Eq. (1).

$$I_{RGB} = \int S_{RGB}(\lambda)R(\lambda)E(\lambda)d\lambda \quad (1)$$

I_{RGB} is observed RGB value. $S_{RGB}(\lambda)$ is camera sensitivity function. $R(\lambda)$ and $E(\lambda)$ are reflectance and illumination spectra, respectively.

The reflectance spectra of thin film $R(\lambda)$ is defined by

$$R(\lambda) = \left| \frac{r_{12} + r_{23}e^{i\Delta}}{1 + r_{23}r_{12}e^{i\Delta}} \right|^2 \quad (2)$$

r_{12} and r_{23} are Fresnel coefficients and represented by Eqs. (3), (4), (5), and (6) for perpendicular and parallel polarization.

$$r_{12}^s = \frac{n_1 \cos \theta_1 - n_2 \cos \theta_2}{n_1 \cos \theta_1 + n_2 \cos \theta_2} \quad (3)$$

$$r_{12}^p = \frac{n_2 \cos \theta_1 - n_1 \cos \theta_2}{n_2 \cos \theta_1 + n_1 \cos \theta_2} \quad (4)$$

$$r_{23}^s = \frac{n_2 \cos \theta_2 - n_3 \cos \theta_3}{n_2 \cos \theta_2 + n_3 \cos \theta_3} \quad (5)$$

$$r_{23}^p = \frac{n_3 \cos \theta_2 - n_2 \cos \theta_3}{n_3 \cos \theta_2 + n_2 \cos \theta_3} \quad (6)$$

Δ in Eq. (2) is phase difference.

$$\Delta = \frac{2\pi\varphi}{\lambda} \quad (7)$$

where φ is an optical path difference determined by a distance between point A and point F in Fig. 1. The distance is $ACF - DF$. Considering a light going into a medium with refractive index n , the light speed in thin film is defined by nc , where c is the light speed in air. Therefore, the optical path difference becomes $n_2ACF - n_1DF$. In Fig. 1, n_1 is the refractive index in air, so $n_1 = 1$. The optical path difference DF is equal to n_2AB .

$$n_2ACF - DF = n_2BCF \quad (8)$$

The optical path difference BCF is equal to $BCF' = 2d \cos \theta_2$ since F' is symmetrical point F .

$$\varphi = n_2BCF = 2dn_2 \cos \theta_2 \quad (9)$$

Therefore, in Eq. (2), zenith angle θ_1 , refractive indices n_2 , n_3 , and film thickness d are important parameters for appearances.

4. Reconstructions with RGB Images

In this section, we propose a method to reconstruct shapes and appearances of thin film objects. First, we propose a shape reconstruction method based on polarization and reflectance intensity analysis of thin film. Second, we propose an appearance reconstruction method.

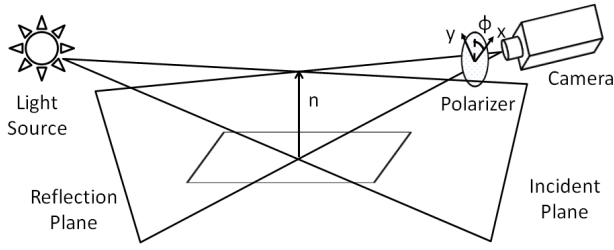


Fig. 2 Relation between incident plane and azimuth angle. x and y are coordinates in camera view. ϕ is rotation angle at perpendicular polarization.

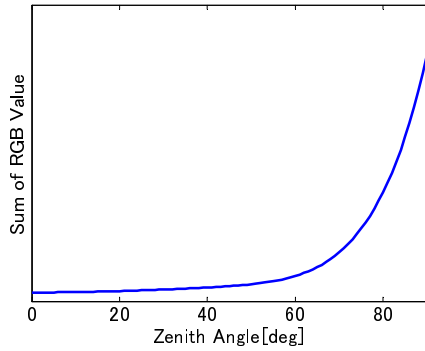


Fig. 3 Sum of RGB values along zenith angle. The refractive index of thin film is 1.36 and that of bottom layer is 1.6. Film thickness is 400 nm. Sensitivity of the camera is EOS 5D [13]

4.1 Polarization

Light has the characteristics of an electromagnetic wave. The polarization of reflected light can be divided by parallel and perpendicular polarization. The parallel polarization is parallel light along the incident plane and the perpendicular polarization is vertical light along the incident plane. As shown in Fig. 2, the azimuth angle is vertical along the incident plane and the perpendicular polarization is parallel to the azimuth angle.

4.2 Zenith Angle

We focus on two features to estimate zenith angles. The first is the degree of polarization (DOP), which can narrow down candidates to two zenith angles. The second is the intensity of perpendicular polarization, which monotonically increases as shown in Fig. 3. In this section, we describe a method to estimate zenith angles using these two features.

When the polarizer is rotated, the observed intensity is changed along the rotating angle. We can obtain the degree of polarization (DOP) by using the maximum and minimum intensities among polarized images, as shown in Fig. 4. DOP is represented as

$$\rho = \frac{I_{max} - I_{min}}{I_{max} + I_{min}} \quad (10)$$

The I_{max} and I_{min} can be theoretically defined as amplitude of Fresnel reflection and transmittance as

$$I_{max} = I_S = (R_s(t) + T_s(t)R_s(b)T_s(b))I \quad (11)$$

$$I_{min} = I_P = (R_p(t) + T_p(t)R_p(b)T_p(b))I \quad (12)$$

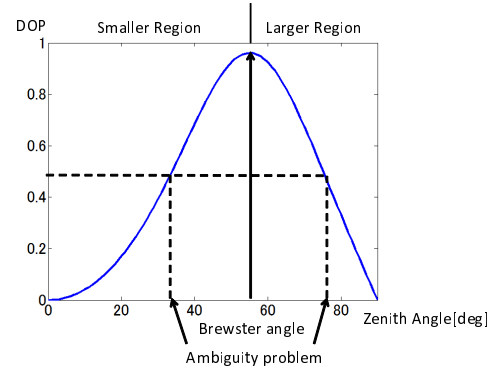


Fig. 4 Degree of polarization. Refractive indices of thin film and bottom layer are 1.36 and 1.6, respectively.

where $R_s(t)$, $R_p(t)$ are the reflections of the top layer, $R_s(b)$, $R_p(b)$ are the reflections of bottom layer, $T_s(t)$, $T_p(t)$ are the transmittance coefficients of the top layer, and $T_s(b)$, $T_p(b)$ are the transmittance coefficients of the bottom layer.

A schematic diagram of thin film is shown in Fig. 1. The amplitude of the Fresnel reflection and transmittance at the top layer are represented as Eq. (13), (14), (15), and (16). In the case of the bottom layer, the equations can be similar to the top layer's equations. n_1 , n_2 , and n_3 are the refractive index of the incoming medium, thin film, and outgoing medium, respectively. θ_1 is zenith angle. θ_2 is refracting angle. θ_3 is angle of outgoing light transmitting the thin film. In our method, we assume that the incoming medium is air, so $n_1 = 1.0$.

$$R_s(t) = \left| \frac{n_1 \cos \theta_1 - n_2 \cos \theta_2}{n_1 \cos \theta_1 + n_2 \cos \theta_2} \right|^2 \quad (13)$$

$$R_p(t) = \left| \frac{n_2 \cos \theta_1 - n_1 \cos \theta_2}{n_2 \cos \theta_1 + n_1 \cos \theta_2} \right|^2 \quad (14)$$

$$T_s(t) = \frac{\tan \theta_1}{\tan \theta_2} \left| \frac{2 \sin \theta_2 \cos \theta_1}{\sin(\theta_1 + \theta_2)} \right|^2 \quad (15)$$

$$T_p(t) = \frac{\tan \theta_1}{\tan \theta_2} \left| \frac{2 \sin \theta_2 \cos \theta_1}{\sin(\theta_1 + \theta_2) \cos(\theta_1 - \theta_2)} \right|^2 \quad (16)$$

Here, we can calculate the DOP along the zenith angle if we know the refractive index of the thin film and bottom layer.

In Fig. 4, the refractive indices of the thin film and bottom layer are 1.36 and 1.6, respectively. The vertical axis is the value of DOP and the horizontal axis is the zenith angle from 0 to 90 degrees. As shown in Fig. 4, the DOP has two solutions across the Brewster angle.

To solve before the ambiguity, we came up with the following method. We can divide by two regions, e.g., a "larger region" and a "smaller region". The larger region has a larger angle than the Brewster angle and the smaller region has a smaller one. The intensity of perpendicular polarization can be calculated from Eqs. (11), (13), and (15). When the intensity becomes larger than that of the Brewster angle, we can determine that region as the larger region and can then detect the zenith angle in the larger region. The reverse is true when the intensity is smaller than that of the Brewster angle.

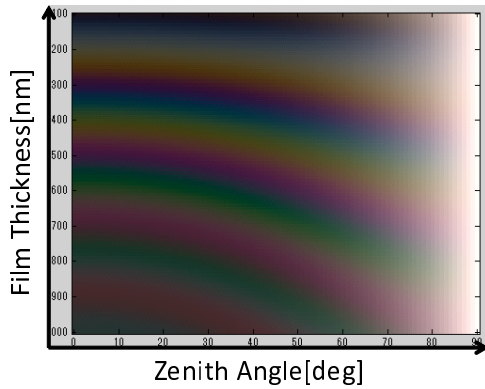


Fig. 5 Simulated appearance along zenith angle and film thickness. Zenith angle is from 0 to 90 degrees. Film thickness is from 100 nm to 1000 nm. The refractive index of thin film is 1.36 and that of the bottom layer is 1.6.

4.3 Azimuth Angle

We can estimate azimuth angles by using perpendicular polarization. We detect rotation angles observing perpendicular polarization and estimate azimuth angles. When the polarizer is rotated, the intensity of captured images is changed from bright to dark among a 180° polarizer rotation. As mentioned in the previous section, azimuth angle is parallel to perpendicular polarization. Therefore, the rotation angle is equal to azimuth angle when we observe maximum intensity. However, there are two maximum intensities. If we define one angle as ϕ , the other one becomes $\phi + 180^\circ$. We can solve this ambiguity by using the occluding boundaries of the target object.

Then, we assume that surface normal directs outwards. When the boundary is closed, the integrated value of surface normal in a small region becomes 0. [9]:

$$\iiint_C f(x, y, z) dx dy dz = 0 \quad (17)$$

where C is the small region area on target objects. We estimate azimuth angles of whole objects with the following steps.

- (1) Estimate azimuth angles of occluding boundaries assuming that all azimuth angles of boundaries direct outwards.
- (2) Estimate azimuth angles near the boundary satisfying Eq. 17.
- (3) Estimate azimuth angles in whole region of target objects by applying step 2 to all pixels.

4.4 Procedure for Appearance Reconstruction

In this section, we propose a method to estimate film thickness. When we know the refractive index of a thin film, we can simulate the appearance along the zenith angle and film thickness by using Eq. 2. As shown in Fig. 5, the appearance can be determined uniquely for the zenith angle and the film thickness. However, we can observe a similar appearance repeatedly along the film thickness. When we input the appearance at a certain zenith angle and take the least square minimum between observed appearance and simulated appearance, we can find the local minimum along the film thickness. Therefore, we need to know the rough range of the film thickness in advance.

Table 1 Estimated Thickness and RMSE of Measured Reflectance

Zenith angle [deg]	Estimated thickness [nm]	RMSE[%]
10	629	1.20
15	618	1.44
20	630	1.05
25	632	0.87
30	628	0.99
35	624	1.45
40	626	1.18
45	639	1.13
50	661	1.31

5. Experiment with RGB Images

In this section, we investigate the validity of our method by simulation. We also verify the effectiveness of our method with real objects.

5.1 Simulation

We investigated the accuracy of the film thickness estimation and found that the accuracy of azimuth angles depends on the detection accuracy of the rotation angle of the polarizer. The accuracy of the rotation angle has previously been evaluated [24][19][20], so in this section, we examine only the accuracy of the film thickness estimation. We use reflectance spectra measured with a spectrometer as input data. We put the target object and light source on a rotation table and changed the zenith angle from 10 to 50 degrees in 5-deg increments. The material used for the thin film is MgF_2 with a refractive index of 1.36. The material of the bottom layer is a PET film with a refractive index of 1.6. The ground truth of film thickness is 630 nm. Tab. 1 shows the estimated film thickness. The average error is 6.56 nm. At 15 and 50 degrees, the error is over 10 nm.

5.2 Measurement of Real Object

In this section, we demonstrate the measurement of a few real objects using our equipment. For this experiment, we used a cylindrical object, and a quadrangular pyramid button with MgF_2 evaporated on their surfaces. The bottom layer of the cylindrical object is PET film with a refractive index of 1.6 and film thickness of 400 nm. The planar thin film was rolled up onto the cylindrical object.

The quadrangular pyramid object is made of ABS resin with a refractive index of 1.5. It had MgF_2 directly evaporated on its surface, the film thickness of which was 630 nm. Vacuum coating equipment is generally used for planar objects, but there is no guarantee that film thickness is evaporated uniformly on non-planar objects. However, our method can measure spatial normal and thickness on a non-planar object.

First, we show the estimated results of the zenith angle in Figs. 6. Fig. 6.(b) shows the estimated zenith angle. The middle area of Fig. 6 is facing the hole in the plastic sphere of the geodesic dome. We captured images thorough this hole and then obtained no solution in this area for cylindrical object.

Second, we show the estimated surface normal and its error in Fig. 7. The top row of Fig. 7 shows the results of the cylindrical object. The average error was 4.48 degrees. The bottom row of Fig. 7 shows the results of the quadrangular pyramid object.

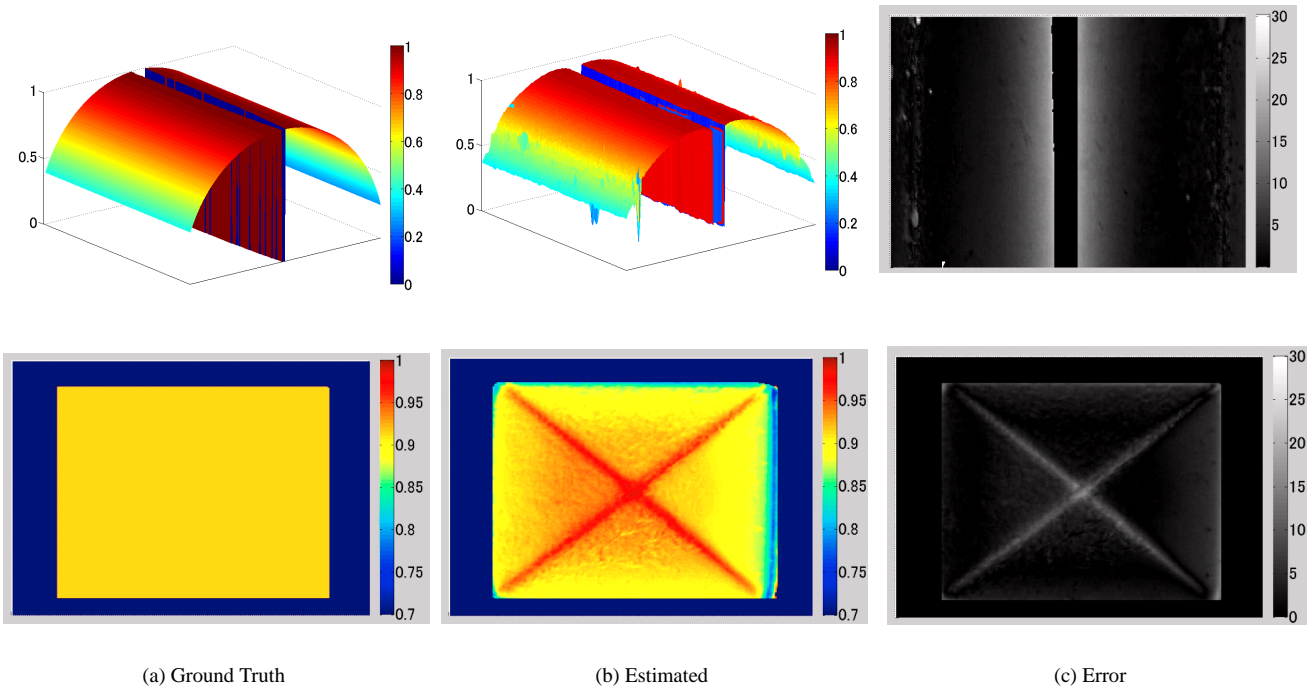


Fig. 6 Estimated results of zenith angle. (a) Ground truth in polar coordinates. (b) Estimated zenith angle in polar coordinates. (c) Estimation error in degrees.

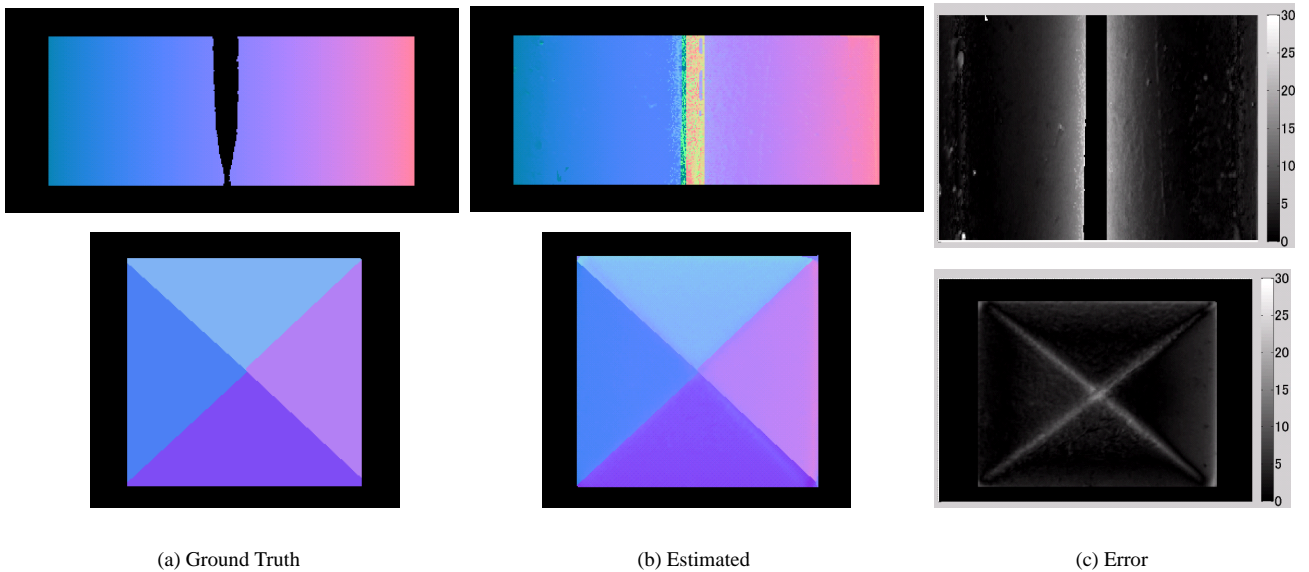


Fig. 7 Estimated results of surface normal. (a) Ground truth. (b) Estimated surface normal. (c) Estimation error in degrees.

The average error was 2.82 degrees. Fig. 7(c) shows the errors of angles between the ground truth and estimated surface normals.

Third, Fig. 8 show the results of estimated film thickness. The thickness is around 400 nm for the cylindrical object. However, the thickness of the quadrangular pyramid object varied greatly from 400 nm to 690 nm.

Finally, we show the reconstructed appearance images using our method in Figs. 9. We evaluated the color difference between captured and reconstructed images. The color difference is defined by Eq. (18) in CIE LAB color space. Tab. ?? shows the

difference level of human perception between two colors.

$$\Delta = \sqrt{\Delta L^2 + \Delta a^2 + \Delta b^2} \quad (18)$$

The color difference of the cylindrical object, 0.64, is perceived as "Slight". The color difference of the quadrangular pyramid, 3.0, is perceived as "Noticeable".

6. Reconstruction with Spectral Images

In this section, we describe a step by step algorithm for estimating the shape and reflectance parameters. First, we estimate the incident angle. Second, we estimate the surface normal from

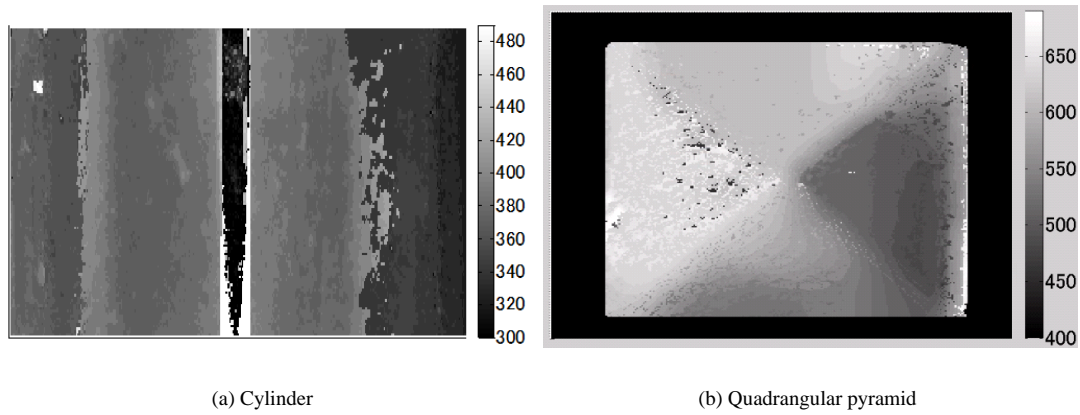


Fig. 8 Estimated results of film thickness.

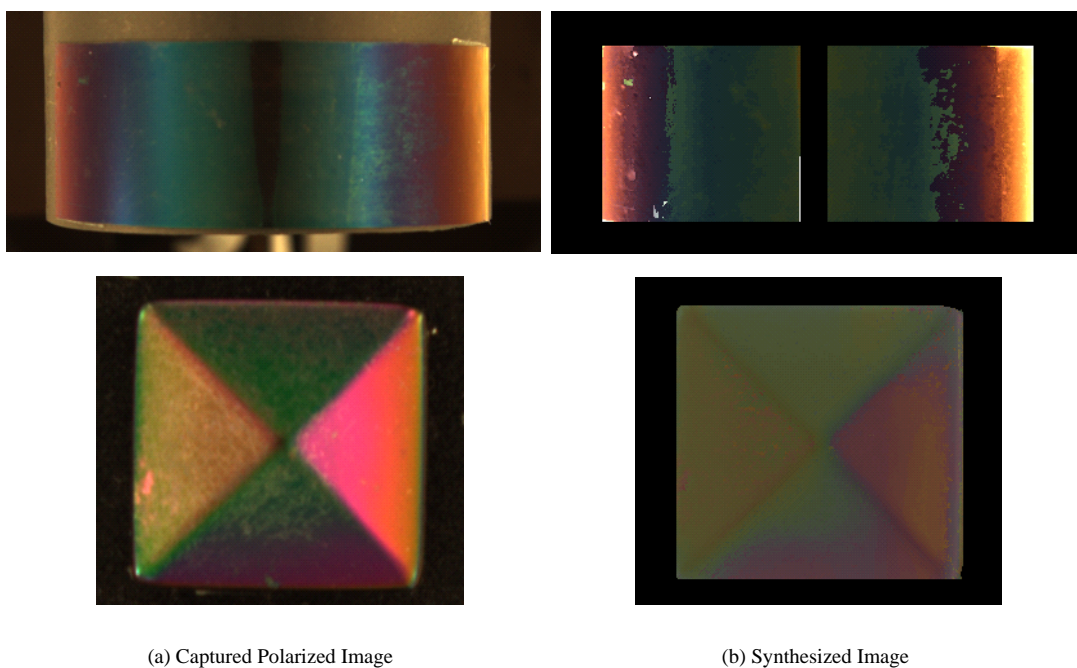


Fig. 9 Captured polarized image and reconstructed image with estimated shapes and film thickness.

the estimated incident angle by using the characteristic strip expansion method. Finally, we estimate the BRDF parameters, such as refractive index and film thickness, from measured reflectance spectra.

6.1 Incident Angle Estimation

We propose an incident angle estimation method, focusing on the monotonically increasing of the "peak intensity" along the incident angle. Fig. 11 shows an example of the peak intensity and peak wavelength enclosed by circles. The local maximum of the reflectance is caused by the full constructive interference. We call this local maximum reflectance "peak intensity" and the wavelength of this local maximum reflectance "peak wavelength".

We find the peak intensity is only dependent on the refractive index of the ground layer, when it becomes higher than the refractive index of the thin film. Fig. 10 shows the peak intensity along the incident angle. Using this monotonically increasing intensity,

we can estimate the incident angle.

The phase difference (Eq. (7)) becomes 2π at the peak wavelength when the refractive index of the ground layer is higher than that of the thin film[17]. Therefore, $e^{i\Delta}$ becomes 1 at this wavelength, so the reflectance intensity at this wavelength $R(\lambda_i)$ can be determined by Eq. (19).

$$R(\lambda_i) = \left| \frac{r_{12} + r_{23}}{1 + r_{23}r_{12}} \right|^2 \quad (19)$$

, where λ_i is the peak wavelength.

Substituting Eqs. (3) and (5) with Eq. (19), the peak intensity of the perpendicular polarization is defined as Eq. (21).

$$R(\lambda_i) = \left| \frac{\cos \theta_1 - n_3 \cos \theta_3}{\cos \theta_1 + n_3 \cos \theta_3} \right|^2 = \left| \frac{\cos \theta_1 - n_3 \sqrt{1 - \sin^2 \theta_3}}{\cos \theta_1 + n_3 \sqrt{1 - \sin^2 \theta_3}} \right|^2 \quad (20)$$

By Snell's law, $n_1 \sin \theta_1 = n_2 \sin \theta_2 = n_3 \sin \theta_3$ and $n_1 = 1.0$, Eq.(7) becomes as follows.

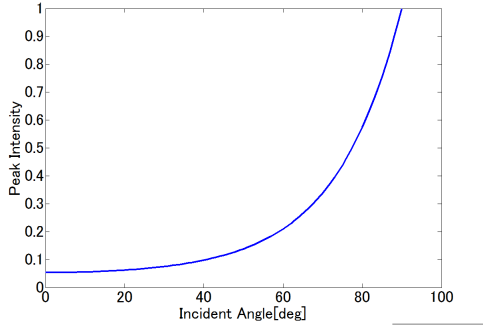


Fig. 10 Peak intensity along incident angle. We calculate intensity with refractive index of the bottom layer of 1.6.

$$R(\lambda_t) = \frac{\left| \cos \theta_1 - n_3 \sqrt{1 - \frac{1}{n_3^2} \sin^2 \theta_1} \right|^2}{\left| \cos \theta_1 + n_3 \sqrt{1 - \frac{1}{n_3^2} \sin^2 \theta_1} \right|^2} = \frac{\left| \cos \theta_1 - \sqrt{n_3^2 - \sin^2 \theta_1} \right|^2}{\left| \cos \theta_1 + \sqrt{n_3^2 - \sin^2 \theta_1} \right|^2} \quad (21)$$

The equation shows that the peak intensity of the perpendicular polarization depends on the incident angle and refractive index of the ground layer. In our method, we assume the refractive index of the ground layer is known. We also verified the integral intensity in the whole visible wavelength and found that it becomes monotonically increasing. However, this intensity depends not only on the refractive index of the ground layer but also on the refractive index of the thin film.

We determine the incident angle domain by minimizing the least square error between the peak intensity Eq. (21) and that of the measured reflectance.

$$\text{Arg min}_{\theta_1} |R_o(\lambda_t) - R_m(\lambda_t)|^2 \quad (22)$$

$R_o(\lambda_t)$ is the measured reflectance at the peak wavelength. $R_m(\lambda_t)$ is calculated by using the known refractive index of the bottom layer.

6.2 Surface Normal Estimation

We estimate the surface normal of the thin film by using the characteristic strip expansion method proposed by Horn[10]. This method uses the monotonically increasing intensity and steepest ascent in the gradient space. As mentioned in previous section, the peak intensity monotonically increases. We find that the peak intensity corresponds to the gradient. We explain about the correspondence below.

In the image coordinate, an object point (x, y, z) is mapped to a pixel (u, v) , for which $u = x$ and $v = y$ under the orthographic projection. If the object surface z is represented as follows,

$$z = f(x, y) \quad (23)$$

, then the surface normal vector is defined by Eq. (24).

$$(p, q, -1) = \left[\frac{\delta f(x, y)}{\delta x}, \frac{\delta f(x, y)}{\delta y}, -1 \right] \quad (24)$$

, where p and q are the parameters of the surface normal. The quantity (p, q) is the gradient of (x, y) and is called the ‘‘gradient space’’.

Normalizing Eq. (24) as 1, the z component of the surface normal becomes

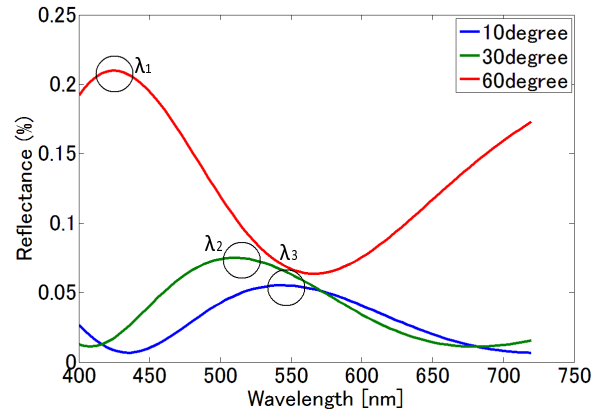


Fig. 11 Reflectance of thin film at 10, 30 and 60 degrees shown as blue, green and red lines respectively. The refractive index of these reflectance is 1.37 and the film thickness is 400 nm.

$$z = \frac{1}{\sqrt{p^2 + q^2 + 1}} \quad (25)$$

This component is also equal to the cosine of the incident angle. Setting $x^2 + y^2 + z^2 = 1$, the existence domain of $f(p, q)$ is on the circumference defined as Eq. (26).

$$p^2 + q^2 = \frac{1}{\cos^2 \theta_1} - 1 \quad (26)$$

By Eq. (26), the existence domein of gradients corresponds to the peak intensity. The peak intensity is determined uniquely by the incident angle. Also the existence domain is defined uniquely by the incident angle as shown in Eq. (26). This correspondence make it able to apply the characteristics strip expansion method to the thin film objects.

We describe the estimation procedure with Fig. 12. Red arrows are steepest ascents in the peak intensity map. Purple arrows are steepest ascent in the gradient space.

- (1) Drawing contour lines by sampling the peak intensity per 0.1
- (2) Start from the pixel (x_1, y_1) in captured image which gradient (p_1, q_1) is known
- (3) Moving to the steepest ascent direction of (p_1, q_1) in captured image and determining (x_2, y_2) as the next pixel where intersect with contour line of the peak intensity
- (4) Moving to the steepest ascent direction of (x_1, y_1) in gradient space and determining (p_2, q_2) as the next gradient where intersect with contour line of the gradient
- (5) Repeating steps 3 and 4 until the whole surface normal is estimated

6.3 Refractive Index and Film Thickness Estimation

The refractive index and the film thickness are important optical parameters for reconstructing the appearance of thin film. We developed a more effective method for estimating these parameters.

By Snell’s law, the optical path difference of Ep. (??) is rewritten as

$$\varphi = 2d \sqrt{n_2^2 - \sin^2 \theta_1} \quad (27)$$

The optical path difference becomes an integral multiple of the peak wavelength.

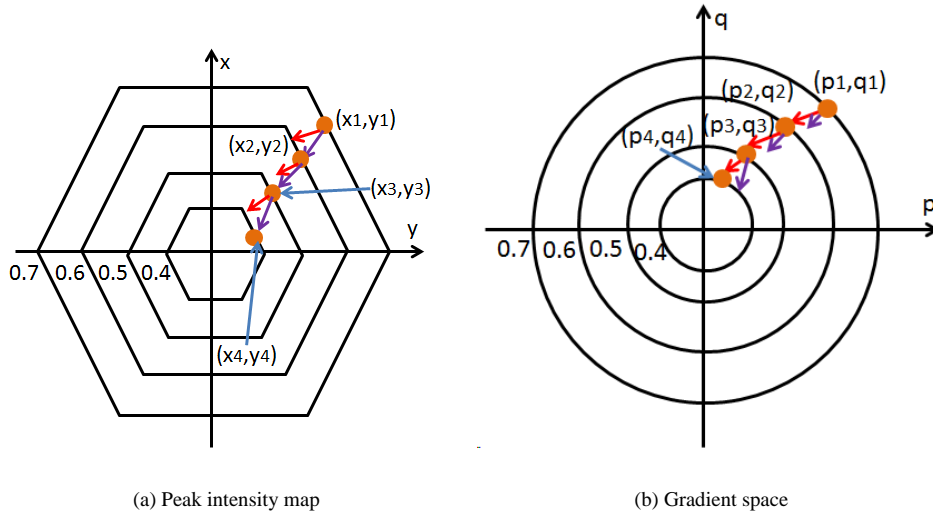


Fig. 12 Example of estimation using the characteristic expansion method. (a) the image which is mapped peak intensity to each pixel. (b) shows contour line in the gradient space.

$$m\lambda_i = 2d \sqrt{n_2^2 - \sin^2 \theta_1} \quad (28)$$

, where m is a natural number. Using Eq. (28), the film thickness is defined as

$$d = \frac{m\lambda_i}{2 \sqrt{n_2^2 - \sin^2 \theta_1}} \quad (29)$$

Therefore, we only need to check the combinations of the refractive index and the film thickness that fit the integral multiples of the peak wavelength. This enables us to reduce the computational time considerably, comparing with that required for the full search.

We determine the refractive index and film thickness by minimizing the square error between the reflectance model and the measured reflectance. The uniqueness of this minimization is guaranteed experimentally. Eq. (30) has some local minima, but it only has global minimum around ground truth.

$$\text{Arg min}_{n_2, m} \left| \sum_{\lambda} R_o(\lambda) - R_m(\lambda) \right|^2 \quad (30)$$

$R_o(\lambda)$ is measured reflectance spectra. $R_m(\lambda)$ is calculated by using the reflectance model in Section 3.

As mentioned in the previous section, the refractive index n_2 is lower than that of the bottom layer. Also, it is higher than 1.0 which is the refractive index in a vacuum. Kobayashi et al.[16] showed that when the refractive index error is approximately 0.01, the color difference of the BRDF becomes sufficiently small. We change the refractive index n_2 by 0.01 from 1.0 to the refractive index of the bottom layer. We then increased the natural number m until the film thickness is less than 1000 nm.

7. Experiment with Spectral Images

We evaluate the accuracy of our method by simulation and real data. For the simulation, we used hemispherical and cylindrical objects. We set the refractive index of thin film to 1.37 and that of the bottom layer to 1.6 which was the same as that of the real

object. We set the film thickness to 400 nm for the hemispherical object and 420 nm to 560 nm along the x-axis for the cylindrical object.

Fig. 13 shows the setup for the thin film reflectance measurement to acquire the real data. A light source was attached to the rotation table to adjust the incident angle. The target thin film was MgF_2 which refractive index is 1.37. The film thickness was 400 nm. The refractive index of the bottom layer was 1.6, made of polyethylene terephthalate. We varied the incident angle from 10 to 42.5 degrees by 2.5 degrees.

The measurement device was a hyper-spectral camera, which consists of a liquid crystal tunable filter (Vari Spec CRI) and a monochrome camera. The liquid crystal tunable filter (LCTF) can change its transmitted wavelengths electrically. The viewing angle of the camera is approximately 30 degrees. The band width in this experiment was 4 nm. We putted a linear polarizer, which transmits S-wave. LCTF also transmits linearly polarized light, so we can capture S-wave reflectance. The transmittance of LCTF is only 4 % around 400 nm. The brightness of S-wave is stronger than that of P-wave, therefore we measure S-wave.

7.1 Incident Angle

Fig. 14 shows the incident angle estimation results of the simulation. Fig. 14 (b) and (e) show the estimated incident angles. Fig. 14 (c) and (f) show the estimation errors. The error increased around 0 to 20 degrees. The error of the spherical object is about 10 degree in this area. In other area, it becomes less than 3 degree. The error of the cylindrical object is about 5 degree in this area. In other are, it becomes less than 3 degree.

Fig. 15 shows the captured reflectance and the estimated result of the real data. The error also increased around 0 to 20 degrees. The error was approximately 9 degrees in this area. At other incident angles, the error was less than 5 degrees.

7.2 Surface Normal

By delimiting the estimated incident angle in Section 7.1 by

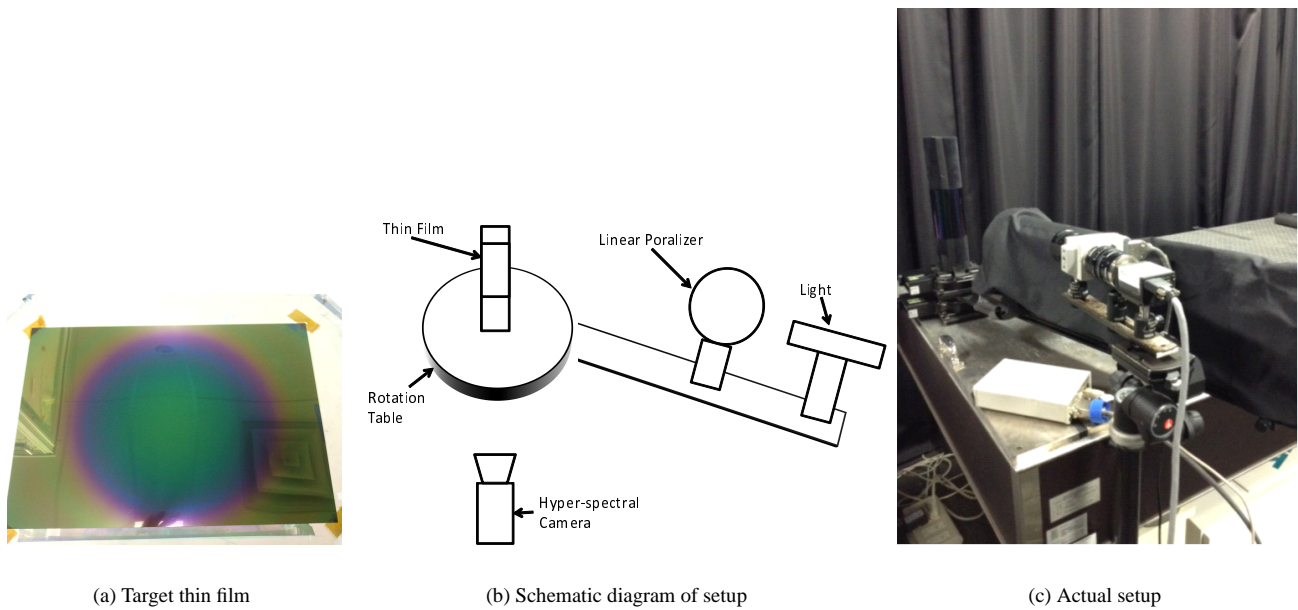


Fig. 13 Experimental setup for measuring thin film reflectance. (a) shows target thin film. (b) shows schematic diagram of setup. (c) shows actual setup. Distance between light source and the thin film was 0.8 m. Distance between the camera and the thin film was 0.6 m.

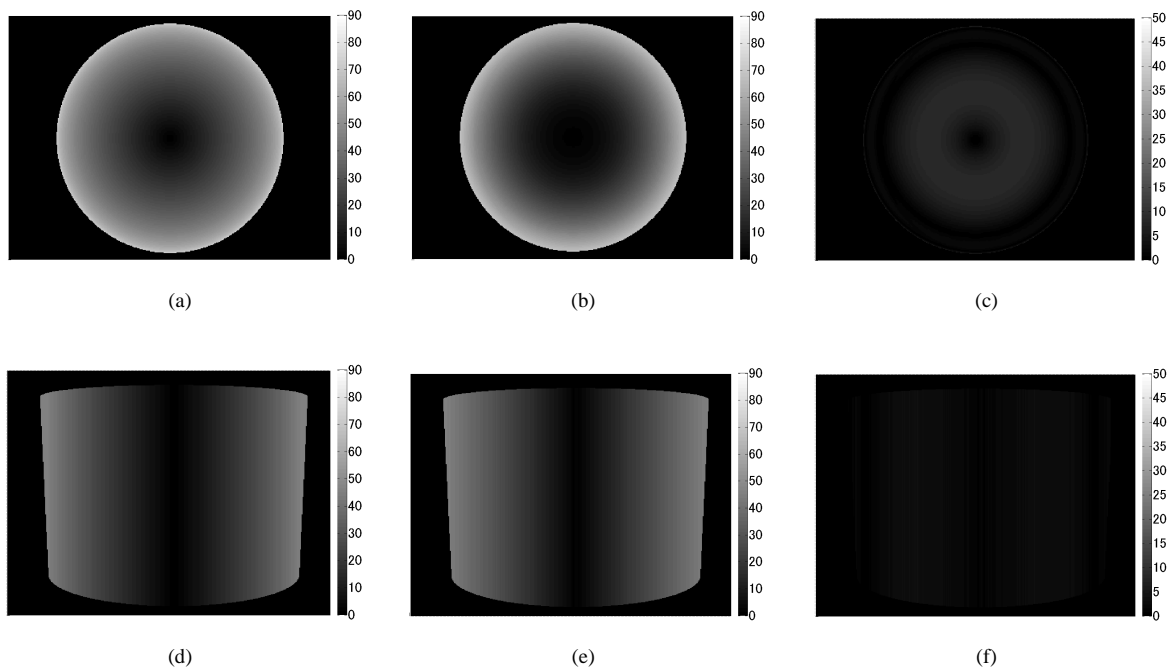


Fig. 14 Incident angle estimation results by simulation. (a) and (d) are ground truths. (b) and (e) are estimated results. (c) and (f) are estimation errors.

3 degrees, we estimated the surface normal by the characteristic strip expansion method. Fig. 16 (b) and (e) show the estimated results.

Fig. 16 (c) and (f) show the estimation errors. The estimation error was calculated as the angle between the ground truth normal and the estimated normal. The maximum error for the hemispherical object was approximately 10 degrees, and that of the cylinder was about 4 degrees. These errors include incident angle errors, then the error of surface normal estimation is about 1

degree. Therefore, the areas in which these errors occurred were the same as the areas where the incident angle errors were large.

7.3 Refractive Index and Film Thickness

We estimated the refractive index and film thickness, by using the estimated incident angle in Section 7.1. For the simulation, the estimated refractive index of the hemispherical and cylindrical objects was 1.37. Fig. 17 (b) and (e) show the estimated film thicknesses. Fig. 17 (c) and (f) show the estimation errors. The

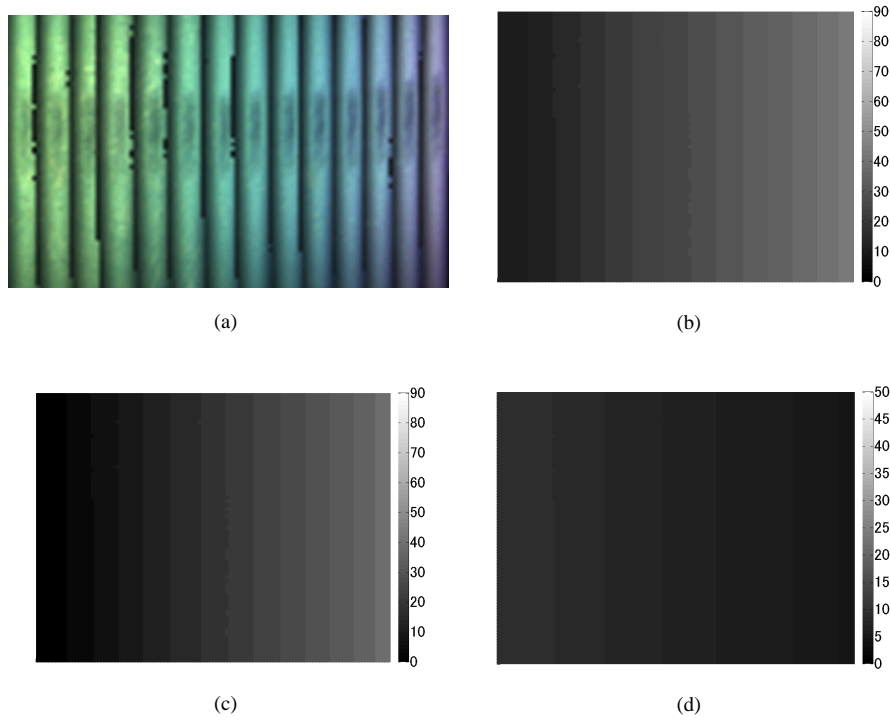


Fig. 15 Incident angle estimation results of real data. (a) shows input reflectance image. (b) shows ground truth incident angle. (c) shows estimated incident angle. (d) shows estimation error.

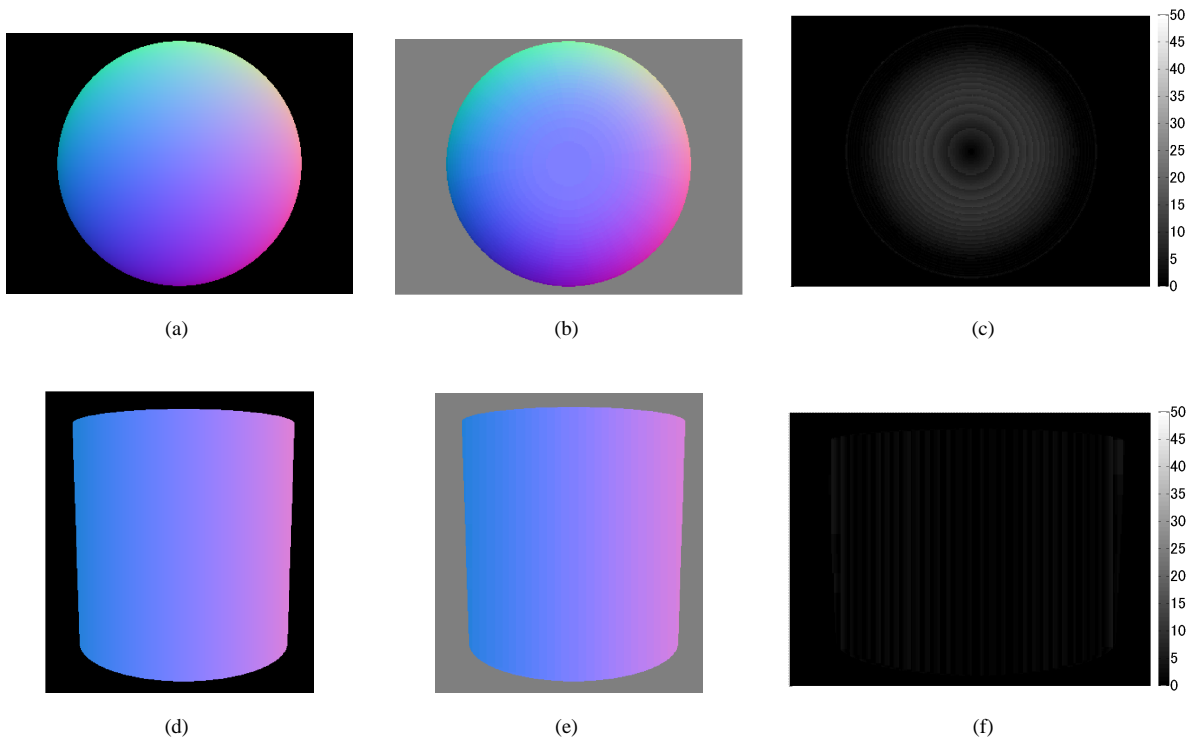


Fig. 16 Surface normal estimation results by simulation. (a) and (d) are ground truth. (b) and (e) are estimated normals. (c) and (f) are estimation errors.

error of the hemispherical object was approximately 10 nm in the area where the error of the incident angle became larger. The error of cylindrical object was about 7 nm in the same area. For the real data, the estimated refractive index was 1.41. Fig. 18 (b) shows the estimated thickness. Fig. 18 (c) shows the estimation

error. The average error was 45 nm.

We calculated the average color difference and root mean square error (RMSE) between the measured reflectance and the reflectance with estimated parameters. The color difference was calculated using Eq. (31).

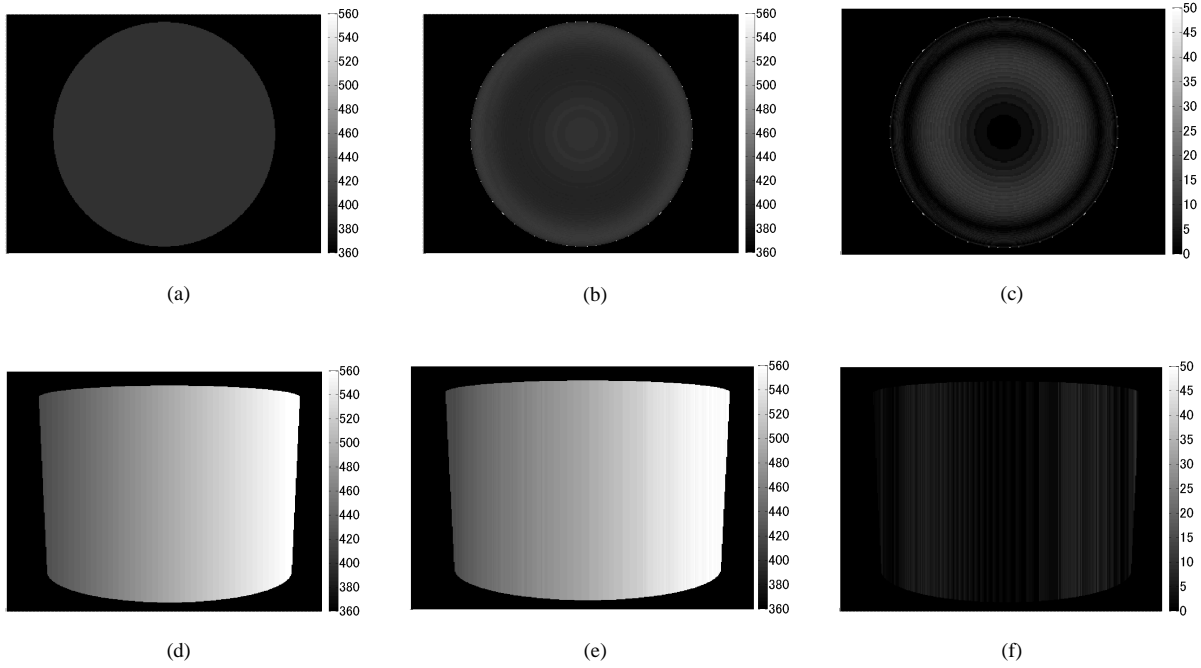


Fig. 17 Film thickness estimation results by simulation. (a) and (d) are ground truths. (b) and (e) are estimated results. (c) and (f) are estimation errors.

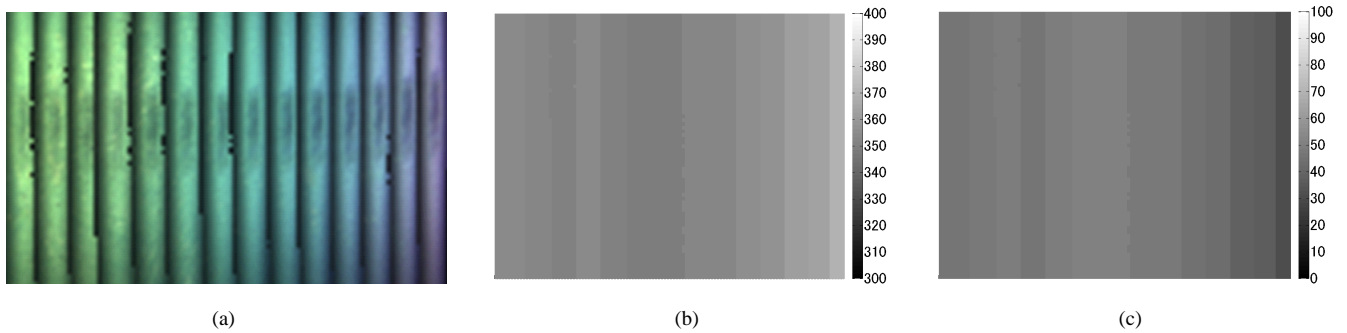


Fig. 18 Film thickness estimation result of real data. (a) shows input reflectance image. (b) shows estimated film thickness. (c) shows estimation error.

$$\Delta E^*_{ab} = \sqrt{(\Delta L^*)^2 + (\Delta a^*)^2 + (\Delta b^*)^2} \quad (31)$$

The RMSE is defined as Eq. (32).

$$RMSE = \sqrt{(R_o(\lambda) - R_e(\lambda))^2 / N} \quad (32)$$

$R_o(\lambda)$ is the measured reflectance. $R_e(\lambda)$ is reflectance calculated by using the estimated parameters. The color difference was approximately 3.33, which can be perceived as a slight difference from the levels given in Table 2. The RMSE was about 2 % for each wavelength intensity.

Fig. 19 shows the rendering results with the estimated surface normal, refractive index and film thickness. Fig. 19 (a) and (b) are the reconstructed appearance of simulation data. Fig. 19 (c) is the image captured by using the hyper-spectral camera and (d) is the synthesized image.

8. Discussion

In this section, we discuss the errors of the simulation and experiment with real objects. First of all, we discuss about errors

Table 2 Level of difference or distance between two Colors

Level of color difference	ΔE^*_{ab}
trace	0 ~ 0.5
slight	0.5 ~ 1.5
noticeable	1.5 ~ 3.0
appreciable	3.0 ~ 6.0
great	6.0 ~ 12.0
very great	over 12.0

with RGB images. First, we examine the thickness error in the simulation. We calculate RMSE between measured reflectance spectra and spectra with ground truth film thickness. RMSE became larger at 15 and 50 degrees, as shown in Table 1. This result indicates that the input reflectance is affected by noise.

We examine the errors of the experiment with real objects. First, we consider that the error is caused by zenith angle error and azimuth angle error. The difference between the zenith angle error in Figs. 6 and surface normal in Figs. 7 is almost the same. Hence, the error of azimuth angle is almost zero.

Second, Fig. 20 shows reflectances of perpendicular and paral-

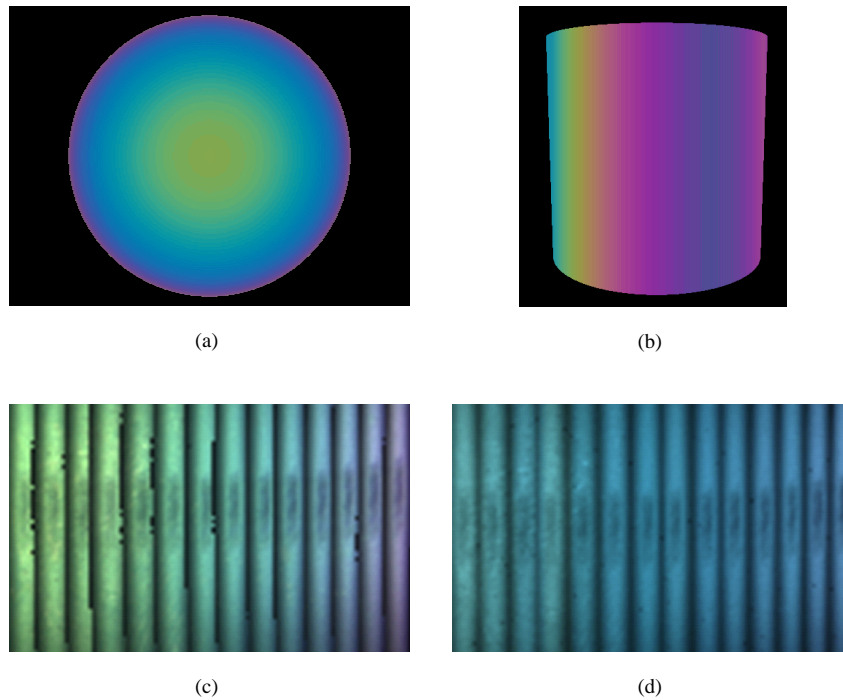


Fig. 19 Image synthesized with estimated surface normal, refractive index, and film thickness. (a) and (b) are results for simulation data. (c) is reflectance image by captured with the hyper-spectral camera. (d) is synthesized reflectance image for real data.

lel polarization along the zenith angle. The optical parameters are the same as Fig. 3. We consider that the error of zenith angles is caused by the noise in input intensity in the lower angle, as shown in Fig. 20. In this area, the difference in angle estimation is quite small with a certain intensity difference. This indicates that the estimated zenith angle is sensitive to noise.

Third, we can recognize the smooth spatial thickness of both objects, but we do not know the ground truth of thickness in Figs. 8. Physical vapor deposition is subject to evaporating thin film: the thinner it is and the farther away from center of the target objects it is. Our results confirm this effect.

Finally, we discuss the difference of the reconstructed appearances in Figs. 9. In our method, we were able to estimate the optical parameters of thin film, such as spatial normal and spatial thickness by a regular digital camera. As shown in Figs. 9, the complex appearance changes of thin film can be represented. In the future, we will discuss how to improve our method for more accurate reconstruction.

Next, we discuss about errors with spectral images. The error of the incident angle became larger around 0 to 20 degrees. In these areas, the peak wavelengths were close to each other. This is very close to the sampling interval of the simulation data and the band width of the hyper-spectral camera, so intensity detection became difficult. The error of the surface normal and optical parameters became large in the same area where the error of the incident angle became large. This error occurred because of the incident angle estimation error. The error of the optical parameters error of the real data becomes large outside these areas. The measured reflectance included noise which make the detection accuracy of the peak wavelength lower. Therefore, we

can avoid these errors by using a high wavelength resolution and hyper-spectral camera with less noise.

Comparing the synthesized image Fig. 19 (d) and real image Fig. 19 (c), we can perceive the difference. The color difference occurs by the error of the incident angle and rounding error of captured reflectance spectra around 430 nm. Over 40 degree, the sample MgF_2 has the peak intensity around 430 nm, but hyper-spectral camera could not capture it with enough brightness because of its low transmittance. The low transmittance cause the rounding error which effects as noise, so we have the difference. The wavelength dependency of the refractive index is also considerable. However, we experimentally verified it does not effect to the estimated appearance for this sample.

We could estimate the incident angle and optical parameters even in darker areas in Fig. 19 (c). In darker areas, just the intensity of the measured reflectance is small, and we could measure reflectance spectra correctly. Therefore, estimated results of Fig. 15 (c) and 18 (b) had parameters in darker areas in Fig. 19 (c).

9. Conclusion

We proposed novel methods for estimating the shape and appearance of a thin film object. The method with RGB images can determine both the shape and thickness of thin film objects using a regular digital still camera and measure the thin film object easily. We also developed the measurement equipment to capture whole reflectance images of thin film objects at once. For the method with spectral images, We found that the peak intensity increased monotonically along incident angle, so we could use the characteristic strip expansion method to estimate the thin film surface normal. We also developed a more efficient method

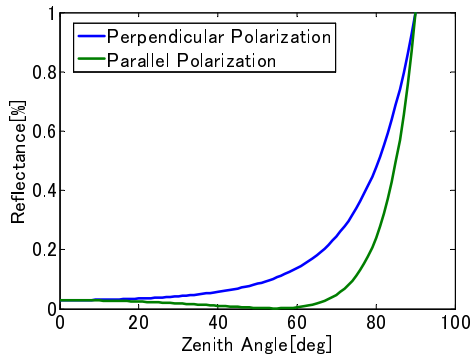


Fig. 20 Reflectance of perpendicular and parallel polarization. Reflectance is the percentage of reflected light from an object.

for estimating the refractive index and the film thickness by using the peak wavelength, where the optical path difference becomes an integral multiple of the peak wavelength. In this paper, our focus was thin film objects with a single layer, but theoretically our method can also be applied to the reconstruction of the shape of multi-layered thin film objects. At the moment, it is difficult to estimate film thickness at each layer of a multi-layered thin film. In the future, we will extend our method to model multi-layered thin film objects.

References

[1] Azzam, R. and Bashara, N.: *Ellipsometry and polarized light*, North-Holland personal library, North-Holland Pub. Co. (1977).

[2] Cuypers, T., Haber, T., Bekaert, P., Oh, S. B. and Raskar, R.: Reflectance Model for Diffraction, *ACM Trans. Graph.*, Vol. 31, No. 5, pp. 122:1–122:11 (online), DOI: 10.1145/2231816.2231820 (2012).

[3] Dana, K. J., van Ginneken, B., Nayar, S. K. and Koenderink, J. J.: Reflectance and Texture of Real-world Surfaces, *ACM Trans. Graph.*, Vol. 18, No. 1, pp. 1–34 (online), DOI: 10.1145/300776.300778 (1999).

[4] Dana, K. J. and Wang, J.: Device for convenient measurement of spatially varying bidirectional reflectance, *J. Opt. Soc. Am. A*, Vol. 21, No. 1, pp. 1–12 (online), DOI: 10.1364/JOSAA.21.000001 (2004).

[5] Herbot, S. and Whaler, C.: An introduction to image-based 3D surface reconstruction and a survey of photometric stereo methods, *3D Research*, Vol. 2, No. 3 (online), DOI: 10.1007/3DRes.03(2011)4 (2011).

[6] Hirayama, H., Kaneda, K., Yamashita, H. and Monden, Y.: An accurate illumination model for objects coated with multilayer films, *Computers and Graphics*, Vol. 25, No. 3, pp. 391–400 (2001).

[7] Hirayama, H., Yamaji, Y., Kaneda, K., Yamashita, H. and Monden, Y.: Rendering iridescent colors appearing on natural objects, *Computer Graphics and Applications, 2000. Proceedings. The Eighth Pacific Conference on*, pp. 15–433 (online), DOI: 10.1109/PC-CGA.2000.883853 (2000).

[8] Holroyd, M., Lawrence, J. and Zickler, T.: A Coaxial Optical Scanner for Synchronous Acquisition of 3D Geometry and Surface Reflectance, *ACM Trans. Graph.*, Vol. 29, No. 4, pp. 99:1–99:12 (online), DOI: 10.1145/1778765.1778836 (2010).

[9] Horn, B. K.: A problem in computer vision: Orienting silicon integrated circuit chips for lead bonding, *Computer Graphics and Image Processing*, Vol. 4, No. 3, pp. 294 – 303 (online), DOI: [http://dx.doi.org/10.1016/0146-664X\(75\)90016-7](http://dx.doi.org/10.1016/0146-664X(75)90016-7) (1975).

[10] Horn, B. K.: A problem in computer vision: Orienting silicon integrated circuit chips for lead bonding, *Computer Graphics and Image Processing*, Vol. 4, No. 3, pp. 294 – 303 (online), DOI: [http://dx.doi.org/10.1016/0146-664X\(75\)90016-7](http://dx.doi.org/10.1016/0146-664X(75)90016-7) (1975).

[11] Imura, M., Oshiro, O., Saeki, M., Manabe, Y., Chihara, K. and Yasumuro, Y.: A Generic Real-time Rendering Approach for Structural Colors, *Proceedings of the 16th ACM Symposium on Virtual Reality Software and Technology*, VRST '09, New York, NY, USA, ACM, pp. 95–102 (online), DOI: 10.1145/1643928.1643952 (2009).

[12] Iwasaki, K., Matsuzawa, K. and Nishita, T.: Real-Time Rendering of Soap Bubbles Taking into Account Light Interference, *Proceedings of the Computer Graphics International, CGI '04*, Washington, DC, USA, IEEE Computer Society, pp. 344–348 (online), DOI:

10.1109/CGI.2004.83 (2004).

[13] Kawakami, R., Zhao, H., Tan, R. and Ikeuchi, K.: Camera Spectral Sensitivity and White Balance Estimation from Sky Images, *International Journal of Computer Vision*, Vol. 105, No. 3, pp. 187–204 (online), DOI: 10.1007/s11263-013-0632-1 (2013).

[14] Kitagawa, K.: Transparent film thickness measurement by three-wavelength interference method: An extended application of Global Model Fitting algorithm, *Mechatronics (MECATRONICS)*, 2012 9th France-Japan 7th Europe-Asia Congress on and Research and Education in Mechatronics (REM), 2012 13th Int'l Workshop on, pp. 94–100 (online), DOI: 10.1109/MECATRONICS.2012.6450993 (2012).

[15] Kitagawa, K.: Thin-film thickness profile measurement by three-wavelength interference color analysis, *Appl. Opt.*, Vol. 52, No. 10, pp. 1998–2007 (online), DOI: 10.1364/AO.52.001998 (2013).

[16] Kobayashi, Y., Morimoto, T., Sato, I., Mukaigawa, Y. and Ikeuchi, K.: BRDF Estimation of Structural Color Object by Using Hyper Spectral Image, *Computer Vision Workshops (ICCVW), 2013 IEEE International Conference on*, pp. 915–922 (online), DOI: 10.1109/ICCVW.2013.125 (2013).

[17] L.S.Pedrotti: *Basic Physical Optics*, SPIE Press Book (2008).

[18] Meinster, K. W.: Interference Spectroscopy. Part I, *J. Opt. Soc. Am.*, Vol. 31, No. 6, pp. 405–426 (online), DOI: 10.1364/JOSA.31.000405 (1941).

[19] Miyazaki, D., Kagesawa, M. and Ikeuchi, K.: Determining Shapes of Transparent Objects from Two Polarization Images, in *IAPR Workshop on Machine Vision Applications*, pp. 26–31 (2002).

[20] Miyazaki, D., Kagesawa, M. and Ikeuchi, K.: Transparent Surface Modeling from a Pair of Polarization Images, *IEEE Trans. Pattern Analysis and Machine Intelligence*, Vol. 26, pp. 73–82 (2004).

[21] Morris, N. J. W. and et al.: Reconstructing the Surface of Inhomogeneous Transparent Scenes by Scatter-Trace Photography (2007).

[22] Mukaigawa, Y., Sumino, K. and Yagi, Y.: Rapid BRDF Measurement Using an Ellipsoidal Mirror and a Projector, *Information and Media Technologies*, Vol. 4, No. 2, pp. 451–462 (online), DOI: 10.11185/imt.4.451 (2009).

[23] Sadeghi, I., Muñoz, A., Laven, P., Jarosz, W., Seron, F., Gutierrez, D. and Jensen, H. W.: Physically-based Simulation of Rainbows, *ACM Transactions on Graphics (Presented at SIGGRAPH)*, Vol. 31, No. 1, pp. 3:1–3:12 (online), DOI: 10.1145/2077341.2077344 (2012).

[24] Saito, M., Sato, Y., Ikeuchi, K. and Kashiwagi, H.: Measurement of surface orientations of transparent objects by use of polarization in highlight, *J. Opt. Soc. Am. A*, Vol. 16, No. 9, pp. 2286–2293 (online), DOI: 10.1364/JOSAA.16.002286 (1999).

[25] Sun, Y., Fracchia, F. D., Calvert, T. W. and Drew, M. S.: Deriving Spectra from Colors and Rendering Light Interference, *IEEE Comput. Graph. Appl.*, Vol. 19, No. 4, pp. 61–67 (online), DOI: 10.1109/38.773965 (1999).

[26] Sun, Y., Fracchia, F., Drew, M. and Calvert, T.: Rendering Iridescent Colors of Optical Disks, *Rendering Techniques 2000*, Eurographics, Springer Vienna, pp. 341–352 (2000).

[27] Wolff, L. and Boulton, T.: Constraining object features using a polarization reflectance model, *Pattern Analysis and Machine Intelligence, IEEE Transactions on*, Vol. 13, No. 7, pp. 635–657 (online), DOI: 10.1109/34.85655 (1991).